Supporting Information

Glycerol-controlled synthesis of series cobalt acid composites and their catalytic decomposition on several energetic materials

Jingjing Wang[a], Suhang Chen[a*], Qiufan Tang[b], Jizhen Li[b], and Kangzhen Xu[a*]

[a] *School of Chemical Engineering/Xi'an Key Laboratory of Special Energy Materials, Northwest University, Xi'an, 710069, China*

[b] *Xi'an Modern Chemistry Research Institute, Xi'an, 710065, China*

Table S1. Solvent ratios of isopropanol and glycerol

Solvent / Ratio	Isopropanol mL	Glycerol mL		Isopropanol mL	Glycerol mL
(12:0)	48	0	(7:5)	28	20
(11:1)	44	4	(6:6)	24	24
(10:2)	40	8	(5:7)	20	28
(9:3)	36	12	(4:8)	16	32
(8:4)	32	16			

It is well known that the crystallinity of the sample has a positive correlation with the catalytic activity. Higher crystallinity will enhance the catalytic performance. Therefore, the crystallization fitting data of MCo_2O_4 composites were obtained by Jade analysis, as shown in **Figure S1**. The crystallinities of MCo_2O_4 (M= Cu, Ni, Zn, Mg, Fe, Ba) composites are 57.0 %, 53.9 %, 56.9 %, 50.0 %, 31.2 % and 57.9 %, respectively. Obviously seen that $BaCo_2O_4$ composite has the highest crystallinity, followed by $CuCo_2O_4$, thus the two may have the better catalytic effect on energetic materials than other MCo_2O_4 (M=Ni, Zn, Mg, Fe) composites.

* Corresponding author. Tel: +86 29 88302632
E-mail address: shchen@nwu.edu.cn (S. Chen)
* Corresponding author. Tel: +86 29 88302632
E-mail address: xukz@nwu.edu.cn (K. Xu)

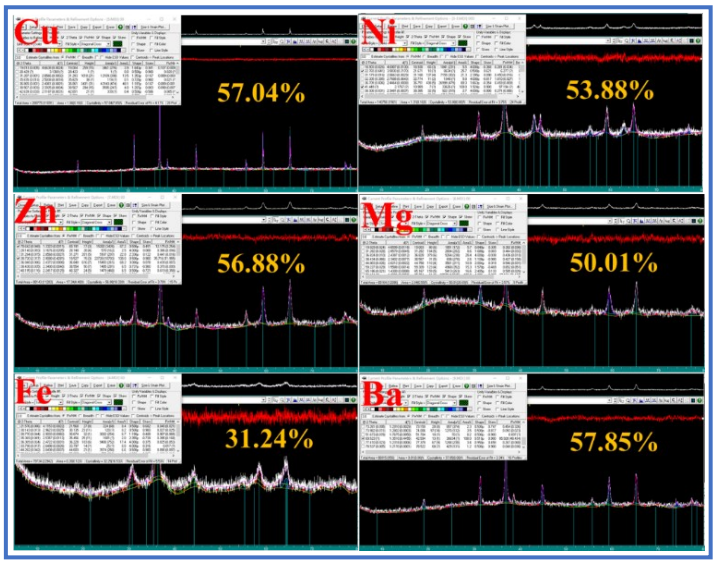

Figure S1. Crystallization fitting data of MCo_2O_4 composites

The elemental composition of MCo_2O_4 composites were tested by EDS and elemental mapping, which indicate the co-existence of C, O, Co and M (M=Co, Ni, Zn, Mg, Fe and Ba) atoms in the samples in **Figure S2**. The elemental mapping results show that distribution of these atoms is uniform on the whole ball. And the atomic ratios of Co and M in MCo_2O_4 composites all closed to 2:1, which were in complete agreement with the standard value of MCo_2O_4, further indicating that the highly purified MCo_2O_4 composites with the similar, uniform and regular morphology were successfully prepared by using the special co-solvent of isopropanol and glycerol.

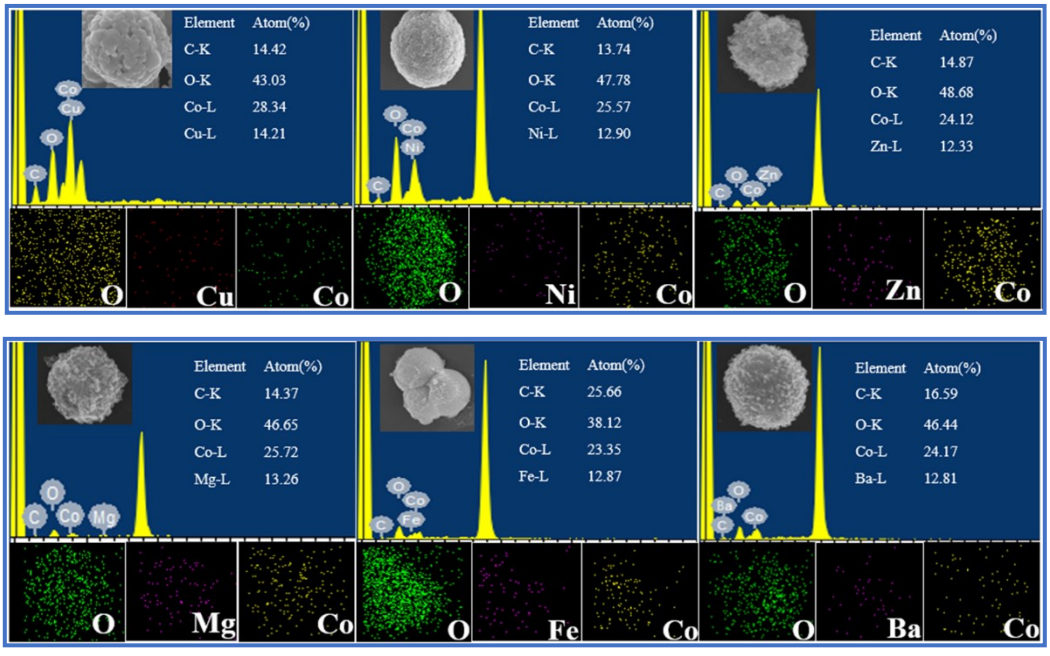

Figure S2. Elemental mapping and EDS images of MCo_2O_4.

Table S2. Mass losses of MCo_2O_4 composites after calcination

Sample	Mass loss %		Mass loss %
$CuCo_2O_4$	42.8	$MgCo_2O_4$	40.6
$NiCo_2O_4$	43.7	$FeCo_2O_4$	42.0
$ZnCo_2O_4$	37.9	$BaCo_2O_4$	40.4

The $MgCo_2O_4$ and $ZnCo_2O_4$ composites were chosen to investigate the porosity and BET surface area by using nitrogen adsorption/desorption instrument (Micromeritics ASAP 2460) and were calculated by a multipoint Brunauer-Emmett-Teller (BET) method. The nitrogen adsorption desorption isotherms were shown in **Figure S3**. The insert in **Figure S3** present the pore size distribution of corresponding samples. The specific surface areas of $MgCo_2O_4$ and $ZnCo_2O_4$ are 17.21 $m^2 \cdot g^{-1}$ and 14.58 $m^2 \cdot g^{-1}$. In addition, $MgCo_2O_4$ and $ZnCo_2O_4$ present typical type IV hysteresis loop and the hysteresis loop of the adsorption-desorption curves in the range of P/P_o of 0.7-1. Pore size distributions embedded in Fig. 6 display the majority of the pore size is ~15.60 nm in diameter for $MgCo_2O_4$ and ~40.20 nm for $ZnCo_2O_4$, which was calculated by the BJH method. The pore size distribution of the $MgCo_2O_4$ composite is narrower than that of $MgCo_2O_4$ as shown in the inset. The higher specific surface area and narrower pore size distribution of $MgCo_2O_4$ can provide more surface activity sites when interacting with AP and RDX, so $MgCo_2O_4$ can exhibit better catalytic performance.

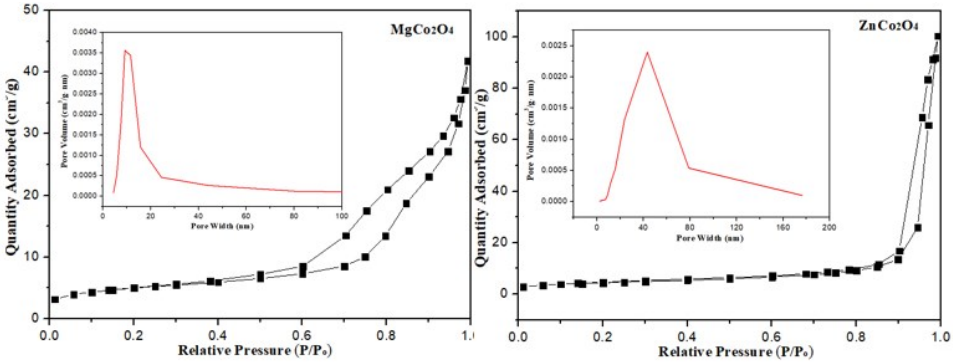

Figure S3. Nitrogen adsorption-desorption isotherms and the corresponding pore size distributions of $MgCo_2O_4$ and $ZnCo_2O_4$.

Figure S4 shows the apparent color images of $NiCo_2O_4$ samples before calcination

with different solvent ratios, and the corresponding yield values are listed at the top of each color map. As shown in **Figure S4**, the color of the $NiCo_2O_4$ (12:0) is light pink, and the yield is 0.4254 g in the solvent of isopropanol. When glycerol was added, the color of the sample changes to khaki. Then, with the increase of glycerol content, the color gradually changes from khaki to light green, and finally turns to dark green (color deepened). Moreover, the yield increases first and then decreases gradually, showing a parabolic trend, and the maximum yield (0.5734 g) appears at the solvent ratio of 9:3. The above results show that the glycerol content has a great influence on the yield and color of the samples from the macroscopic point of view. From the microscopic analysis, glycerol may have some influence on the structure and morphology of the samples, which will be studied and discussed in the next characterization. The conclusion obtained from the above discussion is that the $NiCo_2O_4$ prepared using the special complex solvent of isopropanol and glycerol has the advantages of regular morphology and high yield.

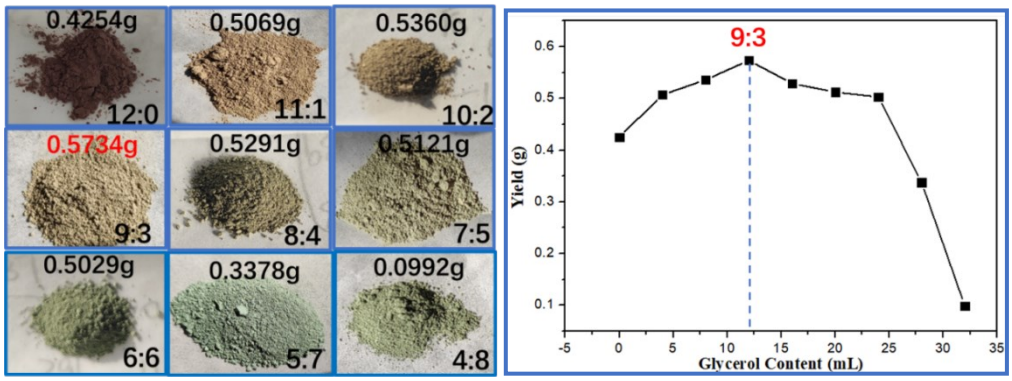

Figure S4. Color images and yield values of $NiCo_2O_4$ composites before calcination under different solvent ratios.

In addition, the quality of $NiCo_2O_4$ (12:0, 11:1, 9:3, 6:6 and 5:7) before and after calcination were recorded and then the mass losses were calculated and presented in **Figure S5**. It can be seen that the mass loss of $NiCo_2O_4$ (12:0) is 33.1 % and with the increase of glycerol content, the mass loss is greater. The results show that the samples synthesized with the special co-solvent of isopropanol and glycerol have higher organic content.

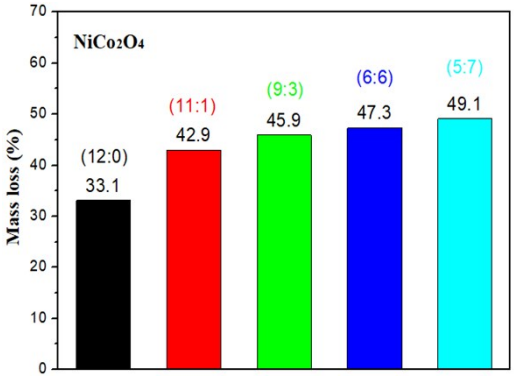

Figure S5. Mass losses of $NiCo_2O_4$ (12:0, 11:1, 9:3, 6:6 and 5:7) after calcination

The XRD results of NiCo2O4 (PVP), NiCo2O4 (urea) and NiCo2O4 (PEG) in **Figure S6** show that $NiCo_2O_4$ composites can also be successfully prepared by using the dispersants of PVP, urea and PEG. In addition, there is also a diffraction peak of NiO (JCPDS 47-1049), indicating that the formation of oxides after calcination in air atmosphere when adding dispersants.

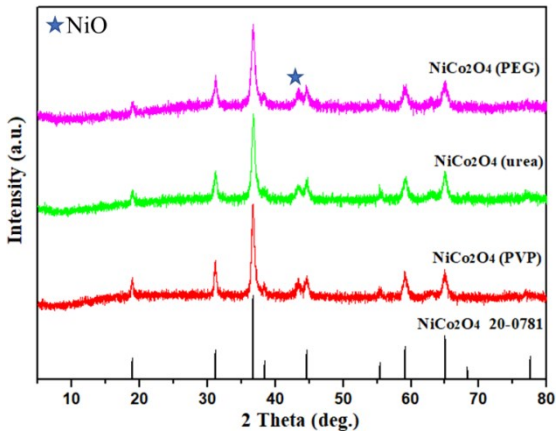

Figure S6. XRD patterns of $NiCo_2O_4$ (PVP), $NiCo_2O_4$ (urea) and $NiCo_2O_4$ (PEG).

Figure S7 and **S8** are the structure and morphology of the mixtures AP+$MgCo_2O_4$ before and after decomposition. The XRD diffraction peaks of AP+$MgCo_2O_4$ before decomposition can match well with the standard card of AP (JCPDS card No. 70-2207) and $MgCo_2O_4$ (JCPDS card No. 81-0667) catalyst, which suggest that the AP+$MgCo_2O_4$ before decomposition contains AP and $MgCo_2O_4$ catalyst. However, for the AP+$MgCo_2O_4$ after decomposition, only the $MgCo_2O_4$ and CoO peaks can be observed in the XRD pattern, indicating that AP has been completely decomposed in the presence of the $MgCo_2O_4$ catalyst. And due to the high temperature of decomposition process, some oxide peaks appear. **Figure S8** reveal that the AP with

the large block structure and the catalysts are mixed uniformly under the mass ratio of 4:1. After decomposition, there are only catalyst and the bulk AP disappears. In agreement with the XRD analysis, AP has been completely decomposed in the presence of catalyst.

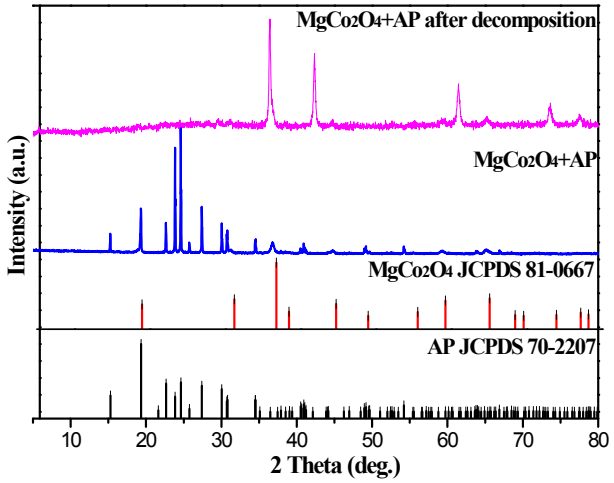

Figure S7. XRD patterns of AP+$MgCo_2O_4$ before and after decomposition.

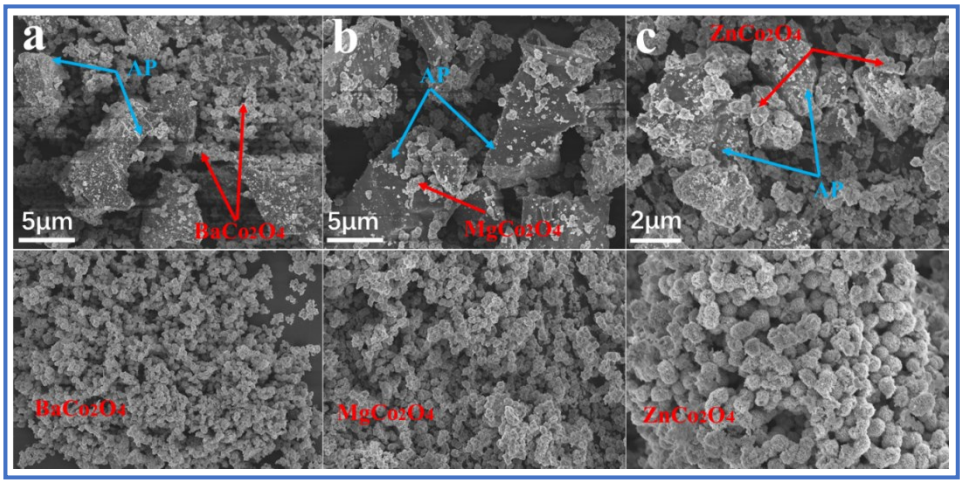

Figure S8. SEM images of AP+$BaCo_2O_4$ (a), AP+$MgCo_2O_4$ (b) and AP+ $ZnCo_2O_4$ (c) before and after decomposition.

The structure and morphology of RDX+$CuCo_2O_4$ before and after decomposition are shown in **Figure S9** and **S10**. The XRD pattern of RDX+$CuCo_2O_4$ before decomposition is correspond well with the standard card of RDX (JCPDS card No. 44-1619) and $CuCo_2O_4$ (JCPDS card No. 78-2177) catalyst, thus indicating the co-existence and uniform admixture of RDX and $CuCo_2O_4$ catalyst. Due to the strange intensity of RDX, the diffraction peaks of $CuCo_2O_4$ are low and not obvious. However, for the XRD pattern of RDX+$CuCo_2O_4$ after decomposition, there is only the

diffraction peaks of $CuCo_2O_4$ and CoO, indicating the complete decomposition of RDX. **Figure S10** shows that the large block structure of RDX and the spherical catalysts are clearly observed, but after decomposition, there are only spherical catalysts. The above results also show that RDX was completely decomposed in the presence of catalysts, which is consistent with the result of XRD characterization.

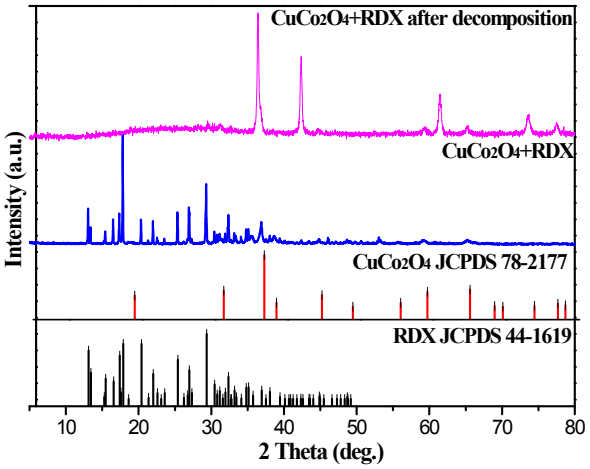

Figure S9. XRD patterns of RDX+$CuCo_2O_4$ before and after decomposition.

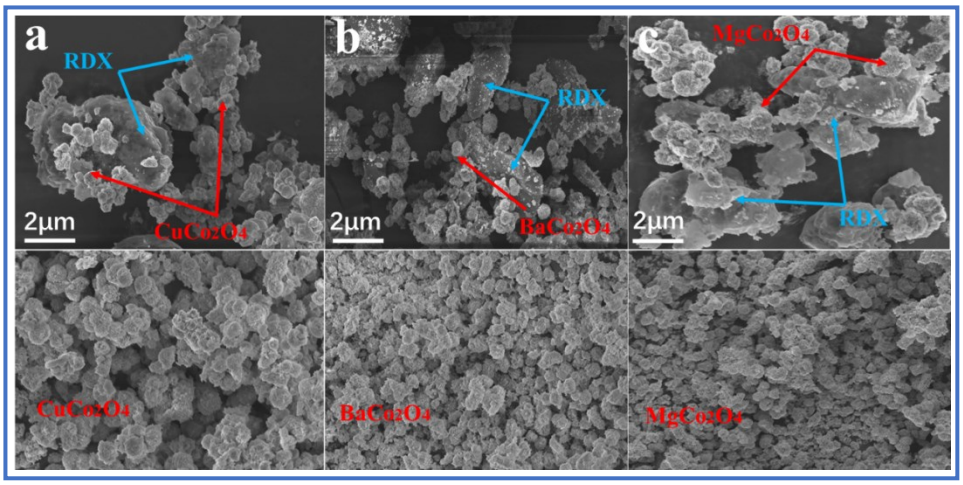

Figure S10. SEM images of RDX+$CuCo_2O_4$ (a), RDX+$BaCo_2O_4$ (b) and RDX+ $MgCo_2O_4$ (c) before and after decomposition.

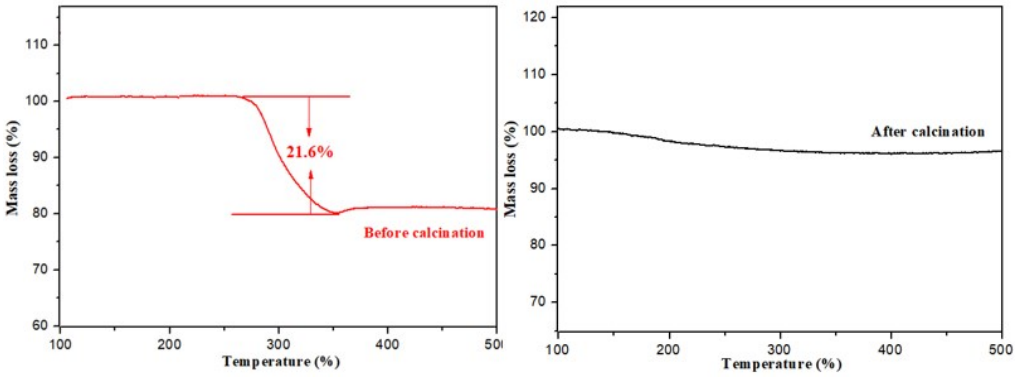

Figure S11. The TG curves of $CuCo_2O_4$ before and after calcination.